Surface & Coatings Technology 294 (2016) 83–89

Contents lists available at ScienceDirect

Surface & Coatings Technology

journal homepage: www.elsevier.com/locate/surfcoat

Formation of three-dimensional nano-trees with perpendicular branches by electrodeposition of CuSn alloy

Tomohiro Shimizu [a,*], Yoshihiro Tada [b], Naoto Kaneko [a], Shukichi Tanaka [c], Shoso Shingubara [a]

[a] Graduate School of Science and Engineering, Kansai University, Yamate-cho 3-3-35, Suita, Osaka 564-8680, Japan
[b] Muroran Institute of Technology, Mizumoto-cho 27-1, Muroran 050-0071, Japan
[c] Advanced ICT Research Institute, National Institute of Information and Communications Technology, Iwaoka 588-2, Kobe 651-2492, Japan

ARTICLE INFO

Article history:
Received 1 October 2015
Revised 8 March 2016
Accepted in revised form 17 March 2016
Available online 25 March 2016

Keywords:
Nanotree
Nanowire
3D nanostructure
Electrodeposition

ABSTRACT

Three-dimensional nano-tree-like structures consisting of single-crystalline CuSn alloy nanowires branching perpendicularly from their parent branches were observed. The nano-trees were formed by constant potential co-electrodeposition of Cu and Sn. The geometry of the branches had a four-fold symmetry around the parent branch, which originated from the crystalline structure of the mother CuSn crystal. XRD and TEM analysis revealed that the nanowire branches consisted of single-crystalline γ-CuSn with ⟨100⟩ preferred growth directions. The addition of polyethylene glycol (PEG) with a molecular weight of 1000 in the plating bath is essential for the formation of the nano-tree structure. It is speculated that adsorbed PEG molecules on CuSn crystal planes with high Miller indices suppress CuSn alloy deposition, enhancing anisotropic growth of the CuSn crystal to form the nano-tree structure.

1. Introduction

Three-dimensional (3D) framework structures consisting of one-dimensional (1D) nanowires have extremely high surface areas, which is of considerable significance in electrochemical device applications such as photovoltaic cells, batteries, and chemical sensors [1–10]. The structure of the 3D framework enables the realization of both a large sensitive reaction area on the surface and electrical interconnection between this sensitive area and the main sensor circuit. Therefore, the formation of 3D framework structure using self-organization techniques has attracted attention and remains an important issue in the realization of high-performance electrochemical devices. Only a few studies investigating the formation of nano-scale 3D framework structures using a one-step self-organization process have been reported, and these have involved, for example, 3D tungsten oxide nanowire networks [2,3,11], pine tree nanowires [12,13], nano-scale latticeworks [14–16]. Thus, materials and growth techniques for the formation of 3D framework structures remain limited.

On the other hand, Sn-containing alloys are one of the most widely used solder materials due to their low melting temperature and low resistivity [17]. However, it is well known that Sn can form 1D crystals called whiskers [18,19]. Sn alloy whisker growth has been considered a serious reliability problem because it causes electrical short-circuits between adjacent electrodes on printed circuit boards after solder application [20]. Such unwanted therefore, the studies of Sn alloy electroplating for solder application have mainly been focused on avoidance of unwanted whisker and dendrite growth using suitable bath additives and composition [18,21]. However, there have been a few studies describing the formation of 2D and 3D nanostructures of CuSn alloys by self-organization [22–24].

During our recent study of CuSn alloy electrodeposition for soldering applications, we unexpectedly discovered the formation of 3D nano-tree-like structures under specific deposition conditions. The oxide of 3D nano-structures containing Sn, which possess high surface area, is potentially promising a candidate for high sensitivity gas sensor [25–27]. In this paper, the growth of CuSn nano-trees is demonstrated using co-electroplating of Cu and Sn, and morphology and crystal structure of the nano-trees are described.

2. Sample preparation

We electrodeposited Cu—Sn alloys on 200-nm-thick sputtered Pt films on Si substrates. Prior to electrodeposition, the Pt surface was cleaned with isopropanol and deionized water in an ultrasonic bath. The Cu—Sn nano-trees were prepared using a Cu—Sn alloy plating bath containing 0.1 M·$SnCl_2$, 0.01 M·$Cu(NO_3)_2$, 0.6 M·$(NH_4)_2C_2O_4$, and poly-ethylene glycol (PEG1000) using a DC electrodeposition method with a potentiostat. The $SnCl_2$ and $Cu(NO_3)_2$ are used as sources of the Sn and Cu ions, and the $(NH_4)_2C_2O_4$ is added as a complexing agent. Formation of ammonium cupric oxalate and stannous oxalate are expected by addition of ammonium oxalate in the CuSn plating bath. Ag|AgCl and a platinum electrode were used as a reference electrode and counter electrode in the electrochemical cell, respectively. A

* Corresponding author.
E-mail address: shimi@kansai-u.ac.jp (T. Shimizu).

http://dx.doi.org/10.1016/j.surfcoat.2016.03.046
0257-8972/

Si substrate with a 200-nm-thick Pt coating was used on a rotating disc electrode as the working electrode. The area of electrode on the rotation disc was 0.61 cm^2. The rotation speed of the disc was maintained at 50 rpm. Cu—Sn alloys were deposited at −0.6 V with respect to Ag|AgCl. The Cu—Sn bath conditions were controlled at 55 °C and a pH of 3.5 during the electrodeposition.

Cyclic voltammetry (CV) measurements were carried out in the potential range between 2.0 V and −3.0 V vs. Ag|AgCl. The sweep rate of the potential was 100 mV/min.

The morphology of the electrodeposited CuSn alloy was observed by scanning electron microscopy (SEM: JEM-7500F, JEOL) with an energy dispersive X-ray analysis (EDX) measurement system, and the crystal structures and atomic ratios of the deposits were analyzed by transmission electron microscopy (TEM: JEM-2100F, JEOL) with an EDX measurement system. The TEM specimens were prepared on carbon-coated Cu meshes. The Cu—Sn alloy electrodeposits were detached from the substrate and cut into small pieces using an ultrasonic bath with deionized water. A drop of the solution containing these cut samples was added to a C-coated Cu mesh and dried in vacuum.

3. Results and discussion

Fig 1 (a)–(c) show SEM images of Cu—Sn alloy samples deposited on Pt electrodes using DC electrodeposition at a constant potential at −0.6 V with the addition of 50 ppm PEG. The duration of electrodeposition was 180 min. The shape of deposits looked like nano-trees with many perpendicular branches, as shown in Fig. 1. Each branch had a 1D structure with a diameter of a few tens of nanometers and grew perpendicularly from the parent branch. Thus, the nano-trees had a 3D hierarchical structure composed of 1D nanowires. Although the overall shape of nano-trees indicated traces of pyramidal growth in tilted view as shown in Fig. 1(b), the side view of nano-tree looked as leaf-shaped growth in Fig. 1 (a). The thickness of widest dimension of the nano-tree was about 8 μm at the middle part as shown in Fig. 1 (a). The average height of nano-tree was approximately 25 μm. In the top view of the nano-tree, four-fold symmetrical branches grew perpendicular to the trunk of the tree, as shown in Fig. 1 (c). This implies that the individual nano-trees are single crystals, and the crystal structure of the nano-tree appears to have a four-fold symmetry, such as cubic.

Fig. 2 (a)–(c) show sequential images of a growth process of the Cu—Sn nano-tree deposited at −0.60 V with an addition of 50 ppm PEG. At early stage of the Cu—Sn deposition shown in Fig. 2 (a), isolated needle like deposits without any branching were observed. With increase in the deposition time, the needle like deposits grew further, and the straight needles were observed in Fig. 2 (b). With further increase in the deposition time, formation of the branches on the needles occurred at 432 s in Fig. 2 (c). Thus, growth of the nano-tree started from the individual parent needles. In addition, compared with Fig. 2 (b) and (c), non-vertically grown parent needles became less prominent with increase in the deposition time. This tendency of vertical alignment is more apparent in longer deposition time, i.e. Fig. 1 (a). Only vertically grown nano-trees were observed in longer deposition time, and the growth of non-vertical needles were stopped due to a natural selection during a competition of growth among the needles. It implies a mass-transfer process of the ion in the electrolyte is involved in the growth mechanism of the nano-tree.

To investigate the effect of PEG addition on the morphology of the CuSn deposits, electrodeposition was performed using the CuSn alloy plating solution with various amount of PEG. Fig. 3 (a) shows typical CuSn deposits without PEG additive at a cathode potential of −0.60 V. Instead of nano-trees, rounded quadrangular CuSn pillars were observed. Under all cathode potential conditions from −0.2 to −0.8 V, nano-trees could not be formed, and the morphology of deposits grown without PEG more closely resembled to that of isotropic 3D growth than that of 1D growth. Fig. 3 (b) shows typical CuSn deposits with the addition of 25 ppm PEG. The morphology of deposits resembled to quadrangular pillars shown in Fig. 3 (a) but the surface of them was rougher. It looks like intermediate shape between quadrangular pillars and nanotrees. The morphology of CuSn deposits indicated nanotree shape with addition of 50 ppm PEG at a cathode potential of −0.60 V as shown in Fig. 3 (c). Thus, the addition of PEG plays a very important role in the formation of nano-trees, by enhancing the 1D anisotropic growth of individual branch during electrodeposition. Fig. 3 (d) indicates the CuSn deposits with addition of 500 ppm PEG. Only 2D grown CuSn film and thin walls were observed. The excess addition of PEG suppressed formation of 1D and 3D structure.

The effect of PEG addition on the composition of the deposits was investigated. Table 1 shows the PEG concentration dependence of the Cu/Sn atomic ratio in the deposits. The Cu/Sn atomic ratio was estimated from EDX results measured by the SEM equipment. There was a tendency of a decrease of the Cu/Sn ratio with an increase in PEG concentration.

Fig 4 (a)–(c) show cross-sectional SEM images of Cu—Sn alloy samples deposited on Pt electrodes using DC electrodeposition at a constant potential from −0.59 to −0.61 V. The duration of electrodeposition was 60 min. The shape of the deposited CuSn alloy changed dramatically with very small variations in the cathode potential. At a potential of −0.59 V (Fig. 4 (a)), an array of nano-needles grew almost perpendicularly to the substrate. The height of the needle and its diameter at the bottom were approximately 5 μm and 200 nm, respectively. There were several small branches, which grew at angles of almost 90° from the needle. It is remarkable that nano-trees with many perpendicular branches were formed at −0.60 V, as shown in Fig. 4 (b). Each branch had a 1D structure with a diameter of a few tens of nanometers and grew perpendicularly from the parent branch. When the cathode potential was −0.61 V (Fig. 4 (c)), there were no nano-trees with straight trunks or branches, but there were rounded branching structures. From these observations, we conclude that the conditions required to form CuSn nano-trees have a very narrow window of cathodic potential around −0.60 V.

Fig. 5 shows the cathodic potential dependence of the atomic fraction of Cu to (Cu + Sn) in the electrodeposited CuSn alloy. The concentration of Cu tended to decrease with increasing negative potential because the REDOX potential of the Sn ion was lower than that of the Cu ion. The slope of the voltage dependence of the atomic ratio showed

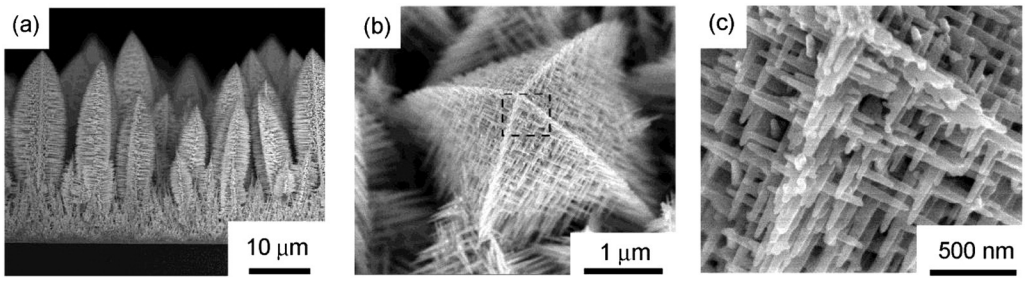

Fig. 1. (a) Cross-sectional view and (b) bird's-eye view SEM images of nano-trees grown by 180 min of long-duration electrodeposition with a cathode potential of −0.60 V. (c) Enlarged image of the nano-tree indicated by the dashed box in (b).

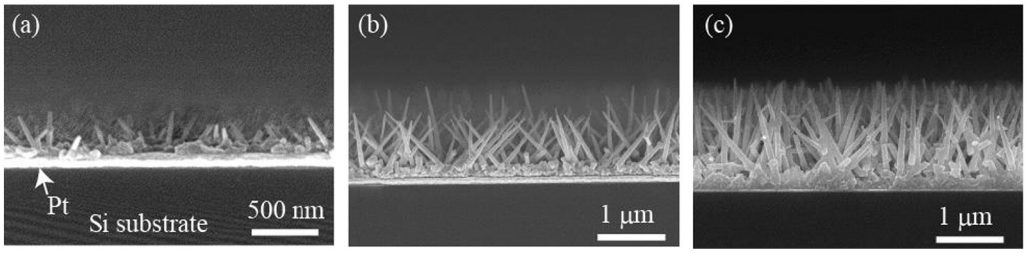

Fig. 2. Cross-sectional view of CuSn alloys deposited at −0.60 V vs. Ag|AgCl for (a) 72, (b) 216 and (c) 432 s.

a distinct change above and below −0.60 V, and there was a flat region around −0.60 V. The Cu—Sn ratio of nano-trees grown at −0.60 V was approximately 81:19.

Fig. 6 shows cyclic voltammetry (CV) curves for Cu and Sn plating bath using Pt electrode as a cathode, respectively. The Cu electroplating solution contained 0.01 M·$Cu(NO_3)_2$, 0.6 M·$(NH_4)_2C_2O_4$, and PEG1000, which was same components as the Cu—Sn alloy electroplating bath except for the Sn source. For the Sn electroplating, the solution containing 0.1 M·$SnCl_2$, 0.6 M·$(NH_4)_2C_2O_4$, and PEG1000 were used. The concentration of PEG in the each solution was fixed at 50 ppm. In Fig. 6, the reduction process initiated at a potential of about −0.1 V vs. Ag|AgCl, which corresponded to the initiation of reduction of Cu^{2+} ions at the cathode surface. The current density of the Cu electroplating solution indicated almost same value in both of outward and return potential sweeps was observed. In contrast, Sn^{2+} reduction process initiated at −0.67 V and clear hysteresis loop was observed. The large oxidation current was observed in the reverse potential sweep, compared with the Cu CV curve.

Fig. 7 shows typical CV curve for Cu—Sn plating bath with and without PEG using Pt electrode as a cathode. The two negative peaks were observed in the both CV curves around −0.55 V and −0.9 V. The Cu deposition process initiated at a potential of about −0.4 V vs. Ag|AgCl. Therefore, at the first negative peak at −0.55 V, the Cu^{2+} reduction was dominant compared with Sn^{2+} reduction, although small amount of Sn^{2+} reduction occurred around this potential. At the −0.7 V, the Sn reduction became dominant, and current indicated negative peak at −0.9 V due to the mass transport limitation of ions. With addition of 50 ppm PEG in the plating solution, the absolute value of current was decreased. Therefore, the PEG in the plating solution worked as an inhibitor for the Cu—Sn plating. In contrast, the oxidation current was increased with the addition of 50 ppm PEG during the revers potential sweep. This could be explained by an increase of Sn ratio in the deposits due to the inhabitation of Cu deposition by PEG.

Fig. 8 shows *I-t* transients for various potential from the Cu—Sn alloy electroplating solution with PEG on Pt electrode. The initial part of each transient is a momentary current due to the charging of the electrochemical double layer. After formation of the electrochemical double layer, the absolute value of the transient currents was decreased. Subsequently, the transient current raised and indicating negative peaks. This increase of *I-t* transient was related to nucleation step of CuSn on the Pt electrode. The formation of nuclei contributes to increase of an active surface area available for ion reduction, and it would increase the *I-t* transient [28]. After the negative peak, the system made transition to the steady–state reaction, controlled by the rate of mass transfer of Cu

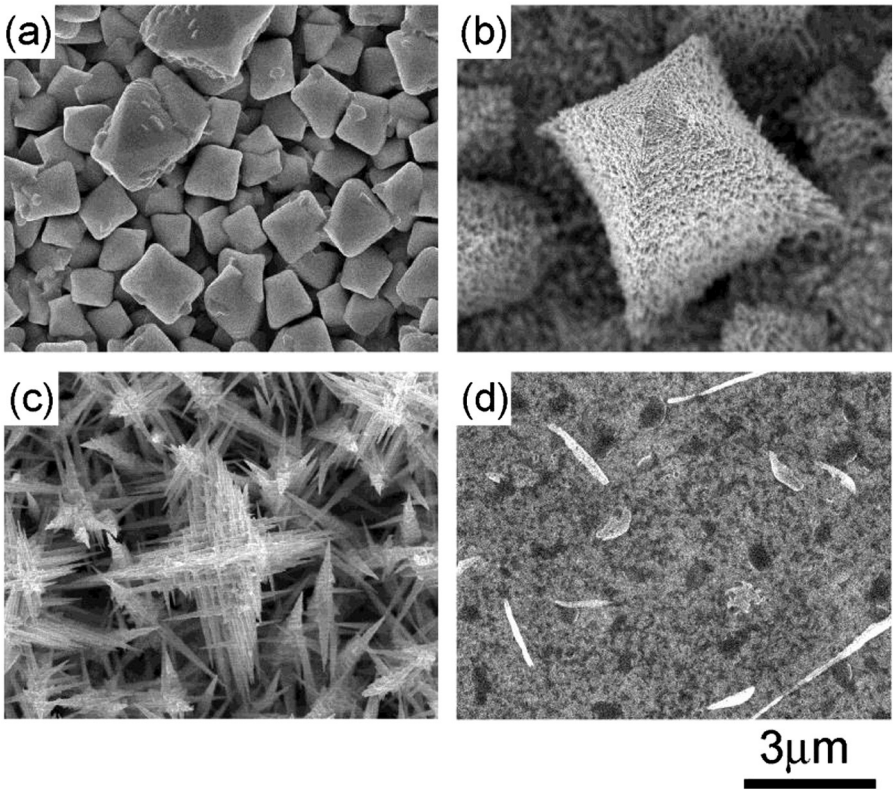

Fig. 3. Top view SEM images of CuSn alloys deposited at −0.60 V vs. Ag|AgCl with various concentrations of PEG additive. (a) Without PEG. PEG concentration of (b) 25 (c) 50, and (d) 500 ppm.

Table 1
Cu/Sn ratio in the deposits electroplated at −0.60 V with respect to Ag|AgCl for 60 min as a function of PEG concentration in the CuSn plating bath.

PEG concentration (ppm)	Cu/Sn ratio
0	5.2
25	4.5
50	4.2

and Sn ion toward the electrode surface. The particular shape of the *I-t* transients for −0.59 and −0.60 V clearly showed that a nucleation process was involved in the electroplating of Cu—Sn alloys. In contrast, the *I-t* transients for −0.61 V did not indicate the negative peak related to the nucleation steps. In addition, the absolute value of the steady state current of −0.61 V was smaller than the others. These would suggest that the Cu—Sn alloy deposits were made without nucleation at −0.61 V, and PEG inhibition of deposition by adsorbed PEG worked stronger than the others.

The cathodic current efficiency, *F* of Cu—Sn alloy deposition was determined by a coulometer and the equation ($F = W_{exp}/W_{theo}$). W_{exp} is the weight of the deposit obtained experimentally, and W_{theo} is the weight of the deposit theoretically according to Faraday's law, assuming the cathodic reactions as reduction of Cu^{2+} and Sn^{2+}. The measurement of W_{exp} was performed with a quartz crystal microbalance using the Cu—Sn alloy solution with PEG for 60 min. The estimated *F* was approximately 0.95 for the cathodic potential at −0.60 V, which was slightly smaller than 1.00. The decrease of *F* from 1.00 was probably attributed to either or both of hydrogen evolution and formation of complex with metal ion and $(NH_4)_2C_2O_4$ because the deposition from complex species is generally not as easy as the deposition from free metal ions [29].

Fig. 9 shows XRD patterns of Cu—Sn deposits on Pt plated at −0.6 V vs. Ag|AgCl, both with and without the addition of 50 ppm PEG. For deposits formed without PEG, a hexagonal closed packed crystal structure considered as ζ-$Cu_{10}Sn_3$ was observed as the main peaks [30,31], in addition to peaks from the Pt electrode and the Si substrate. In the XRD patterns of deposits prepared from plating solutions containing 50 ppm PEG, two new peaks appeared in addition to the ζ-$Cu_{10}Sn_3$ peaks. These additional peaks were from γ-CuSn (110) with a BiF_3-type cubic structure [30,32] and ε-Cu_3Sn (101) with an orthorhombic structure [30,33]. ε-Cu_3Sn is a well-known stable Cu—Sn alloy, as is η-Cu_6Sn_5 at room temperature, according to the equilibrium phase diagram [34]. However, ζ-$Cu_{10}Sn_3$ and γ-CuSn generally exist as high-temperature phases of Cu—Sn alloys in the equilibrium phase diagram. Electrodeposition is known to be a non-equilibrium growth technique. In fact, several papers have already reported the presence of high-temperature phases in Cu—Sn alloys prepared by electrodeposition at room temperature [35,36].

The Cu/Sn atomic ratios of the crystal phases observed in the XRD measurements were 3.0 for ε-Cu_3Sn, 3.3 for ζ-$Cu_{10}Sn_3$, and 2.6 to 5.0 for γ-CuSn, respectively [34]. The Cu/Sn ratio of 5.2 estimated by EDS without PEG shown in Table 1 was too large for ζ-$Cu_{10}Sn_3$ observed in XRD measurement. It seems that the Cu-rich impurities which were not observed in XRD measurements existed in the deposits. Alternatively, there was unknown CuSn phase having a similar crystal structure as the hcp ζ-$Cu_{10}Sn_3$, which was not presented in the equilibrium Cu—Sn phase diagram. In either case, the additional diffraction peaks were observed in the deposits with 50 ppm PEG. The local area EDX measurements were carried out in the TEM equipment for the nanowire of the nano-tree. Fig 10 (a) show TEM image of CuSn nanowire prepared from nano-trees grown with addition of 50 ppm PEG at a cathode potential of −0.60 V. The evaluated Cu/Sn atomic ratio of the nanowire was approximately 4.2, which was almost the same as wide area EDX result measured by SEM shown in Table 1. The estimated Cu/Sn values from EDX measurement were consistent with the composition of cubic γ-CuSn for the sample with 50 ppm PEG. In addition, composition ratio of Cu/Sn was homogenous in the nanowire shown in Fig. 10 (a). Fig. 10 (b) shows selected area diffraction (SAD) pattern of the nanowire. The SAD spots were indexed by assuming a BiF_3-type cubic structure along the [001] zone axis in Fig. 10. In Fig. 10 (b), two weak spots indicated by arrows appeared between the dominant diffraction spots. These weak spots were observed in nanowires grown in ⟨100⟩ directions, and the position of the spots is consistent with the original cubic lattice. It seems that the origin of the weak spots corresponds to a superlattice structure formed in the cubic crystal. Fig. 10 (c) shows a high resolution TEM image of the tip section of the nano-tree shown in Fig. 10 (a). The superlattice structure which corresponds to 3-times of γ- CuSn (220) is confirmed in Fig. 10 (c). The observed branches were single crystal and they grew in the ⟨100⟩ directions. The lattice spacing estimated from the SAD pattern was 0.22 nm for {220}, and 0.15 nm for {400}, and these values agree well with the known lattice spacing of γ- CuSn {220} and {400} for 0.2163 and 0.1529 nm, respectively [30,32].

According to the above results, an individual nano-tree consists of nanowires of γ-CuSn-based single crystals. Moreover, the deposited

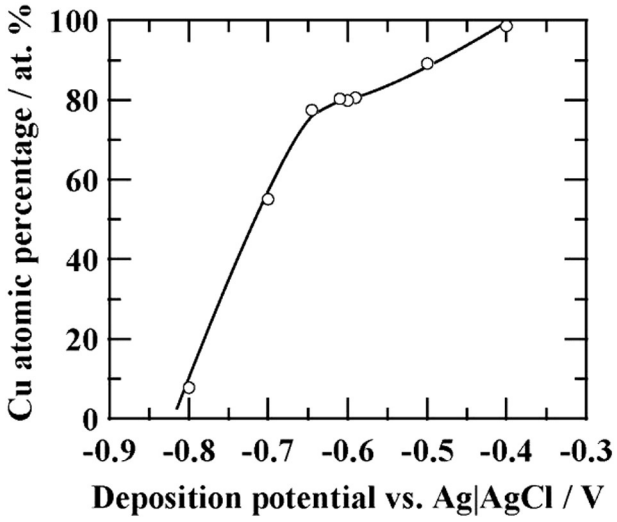

Fig. 5. Potential dependence of Cu atomic percentage in CuSn deposits.

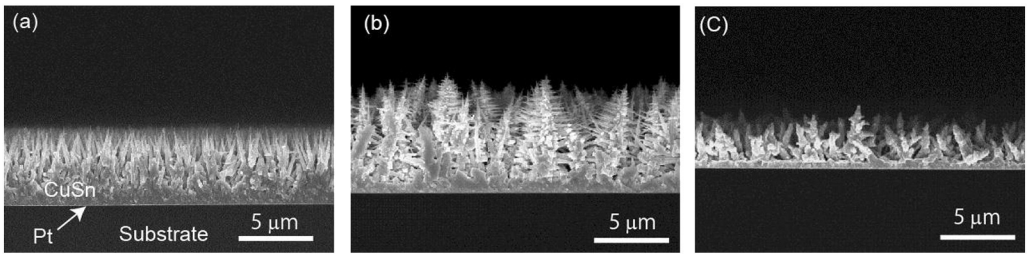

Fig. 4. Cross-sectional SEM images of CuSn alloys deposited at (a) −0.59, (b) −0.60, and (c) −0.61 V vs. Ag|AgCl on a Pt/Si substrate.

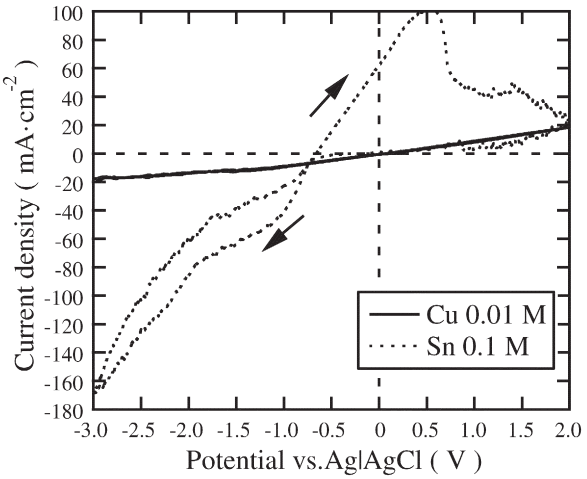

Fig. 6. Cyclic voltammetry curve of Cu and Sn on Pt rotation disc electrode. The arrows indicate sweep direction of potential for Sn.

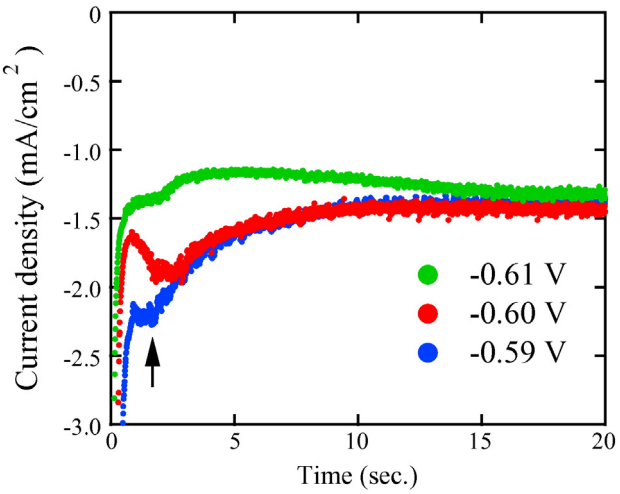

Fig. 8. Current – time (*I-t*) transients during Cu—Sn alloy deposition on the Pt electrode with various potential in the Cu—Sn plating bath containing PEG. The arrow in this image indicates the negative peak observed in the *I-t* transient with the potential at −0.59 V vs. Ag|AgCl.

film under the nano-trees mainly consisted of polycrystalline hcp ζ-$Cu_{10}Sn_3$ which appeared as the main peaks of both samples in the XRD measurements, regardless of the presence of the nano-tree structure. It is presumed that the PEG additive in the plating solution inhibits the growth of a specific crystal orientation of single-crystal γ-CuSn, enhancing the 1D growth of γ-CuSn. The geometry of the nano-trees implies that there are preferred crystal growth directions for nanowires during electrodeposition, which are γ-CuSn ⟨100⟩ indicated in Fig. 9 (b). The six equivalent cubic ⟨100⟩ directions can simply explain the structure of the nano-tree, and each wire grows epitaxially on the mother single-crystal wire.

Mechanisms of branch formation in nanoscale framework structures using self-organization techniques have been discussed in several reports. For example, the growth of an ordered 2D Sn latticework has been explained by periodic potential oscillation during electrodeposition. In particular, the periodic occurrence of three successive processes: autocatalytic growth of a 1D Sn nanowire under diffusion-limited conditions, steady growth of cuboid-Sn crystal under reaction-limited conditions, and autocatalytic surface oxidation of the wires and cuboids, occurred during electrodeposition of Sn in constant-current mode [14]. In contrast, a tungsten oxide nanowire network and a pine tree structure were explained by the presence of crystal dislocations in 1D nanowires that facilitated the nucleation of branching nanowires [11,13]. In our case, a constant potential was applied, and no oscillation of the potential or current was observed during electrodeposition of the CuSn alloy, although both the material system and growth technique were similar to those of the Sn latticework. Therefore, the probable hypothesis explaining the creation of the branched structure in the CuSn alloy is that nanowire surface defects acted as branch nucleation sites [11,13]. There are several possible reasons for the formation of these defects, such as crystal dislocation of the CuSn nanowire or inhomogeneous coating of the PEG molecules acting to inhibit the growth of specific crystal orientations of single-crystal γ-CuSn. To better understanding of nano-tree formation, further TEM observation of the branching points of the nano-trees and detailed investigation of the effects of additives are required. As far as 1D growth of CuSn nanowires with PEG addition is concerned, suppression of CuSn reduction by adsorbed PEG molecules on the CuSn surface seems to be very important as well as mass transfer control of the Cu and Sn ion during electrodeposition. It is known that the addition of PEG in the Cu plating bath inhibits Cu reduction [37,38]. The PEG in Cu electroplating solution react with metal ions on cathodic surface in Cu electroplating solution, forming complex agents of such PEG-Cl-Cu composites. This composition absorbs on active surface of Cu crystal, and works as a diffusion barrier against accumulation of the metal ions [39–42]. Additionally, we also performed the CuSn alloy deposition without Cl in the plating bath using SnC_2O_4 as a Sn source instead of $SnCl_2$, to confirm the effect of Cl for the nano-tree growth. However, we have not observed any nano-trees' formation at any potential even though PEG was added. Bonou et. al. reported the effect of PEG and Cl ion during Cu electroplating on nucleation [42]. They indicated Cu deposition occurred without nucleation with addition of both of PEG and Cl ions,

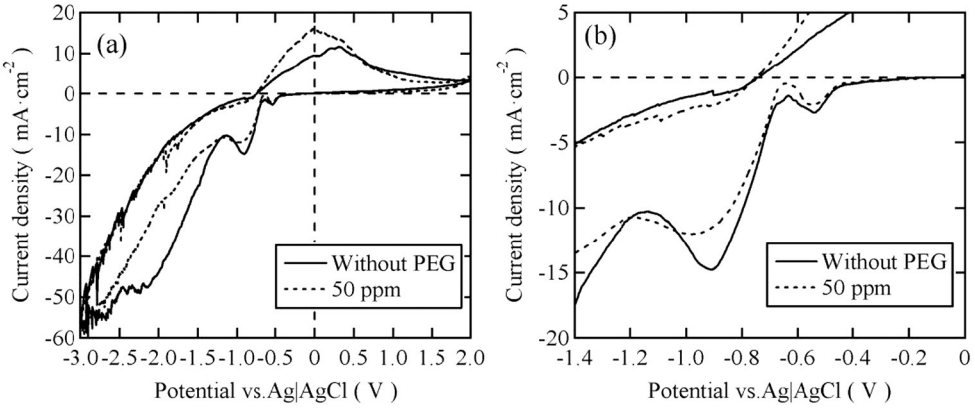

Fig. 7. (a) Cyclic voltammetry curve of Cu—Sn alloy on Pt rotation disc electrode from an Cu—Sn plating bath with 50 ppm of PEG and without PEG. (b) Magnified curve of the potential range from 0 to −1.4 V of Fig. 6 (a).

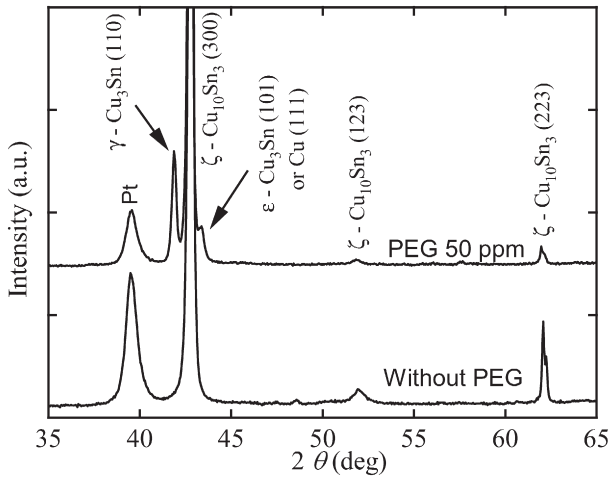

Fig. 9. XRD patterns of Cu—Sn deposits on a Pt electrode plated at −0.60 V vs. Ag|AgCl in plating baths with and without the addition of 50 ppm PEG.

and the surface of the deposited Cu film became smoother than the film plated without PEG and Cl ion. This results suggest that the addition of PEG and Cl ion in the Cu electroplating solution inhibits the three dimensional deposition of Cu on the electrode as well as the deposition rate. In our experiments, the mechanism of the nucleation of CuSn alloy depended on applied potential during the deposition. Therefore, the inhibition of the deposition by PEG and Cl ion began to take effect between −0.60 and −0.61 V in our electroplating condition, which was almost the potential for the growth of nano-trees. Thus, appropriate inhibition of deposition would be necessary for the nano-trees formation. Therefore, it is speculated that adsorbed PEG molecules on specific CuSn crystal planes with high Miller indices suppress CuSn alloy deposition with the help of Cl, as shown in Fig. 11. The PEG adsorbed on the CuSn inhibits metal deposition, and the CuSn does not grow on the surface covered with PEG. A nucleation of branch of the nano-tree may occur at the defect of PEG on the CuSn surface. Then, the electrical field concentrates at the convex parts of the CuSn tips, and enhanced growth of the CuSn at the positon. As a result, anisotropic growth of CuSn nanowires along the ⟨100⟩ direction was occurred by the PEG addition. Moreover, it is known that an addition of PEG in a plating solution suppresses hydrogen gas evolution [43]. The hydrogen gas evolution may affect the morphology of deposits by changing the hydrodynamic conditions in the near-electrode layer [44]. The addition of PEG may contribute to keep the diffusion-limiting condition leading to the formation of the nano-tree.

4. Conclusions

In conclusion, the present work discovered the formation of CuSn nano-trees using a co-electrodeposition technique with PEG, and the detailed nano-tree growth conditions were investigated. Adding PEG

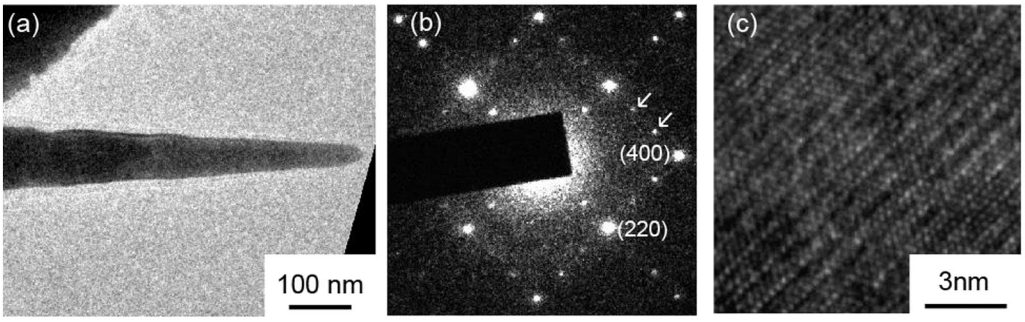

Fig. 10. (a) Bright field TEM image of branches prepared from part of CuSn nano-tree. (b)The SADE patterns of the branch shown in Fig.8 (a). (c)HR-TEM image of Fig. 8 (a).

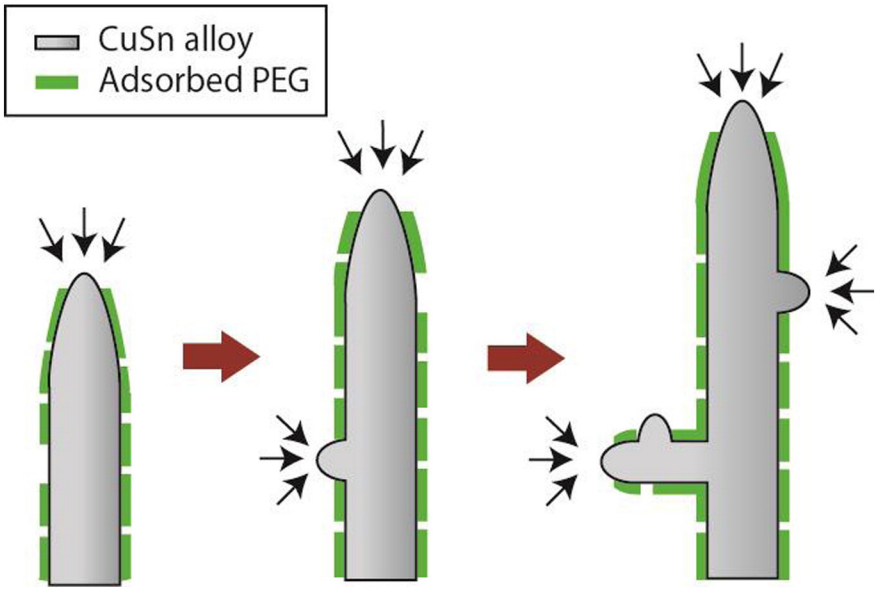

Fig. 11. Schematic of CuSn nano-tree growth mechanism assisted with adsorption of PEG with the help of Cl on the CuSn surface. The small arrows indicate concentration of electrical field. The PEG adsorbed on the specific crystal surface of the CuSn works as inhibitor for metal deposition.

during the electrodeposition of the CuSn alloy is important to obtain CuSn nano-trees. Moreover, each nanowire in a nano-tree consists of a single crystal γ-CuSn, and the growth directions of the branches are ⟨100⟩. The detailed formation mechanism of the nano-tree remains under investigation. In particular, the mechanism of one-dimensional growth of single-crystal γ-CuSn and the branching trigger are essential topics of further study.

Acknowledgements

This work was supported by KAKENHI Grant Numbers 25790024 and 25600048 from the Japan Society for the Promotion of Science (JSPS), Strategic Project to Support the Formation of Research Bases at Private Universities: Matching Fund Subsidy from the Ministry of Education, Culture, Sports, Science and Technology (MEXT), and Kansai University Subsidy for supporting Young Scholars 2013.

References

[1] D.M. Piper, J.H. Woo, S.-B. Son, S.C. Kim, K.H. Oh, S.-H. Lee, Hierarchical porous framework of Si-based electrodes for minimal volumetric expansion, Adv. Mater. 26 (2014) 3520–3525.
[2] A. Ponzoni, E. Comini, G. Sberveglieri, J. Zhou, S.Z. Deng, N.S. Xu, Y. Ding, Z.L. Wang, Ultrasensitive and highly selective gas sensors using three-dimensional tungsten oxide nanowire networks, Appl. Phys. Lett. 88 (2006), 203101.
[3] M. Shibuya, M. Miyauchi, Efficient electrochemical reaction in hexagonal WO_3 forests with a hierarchical nanostructure, Chem. Phys. Lett. 473 (2009) 126–130.
[4] H.R. Kim, K. Il Choi, J.H. Lee, S.A. Akbar, Highly sensitive and ultra-fast responding gas sensors using self-assembled hierarchical SnO_2 spheres, Sensors Actuators, B Chem. 136 (2009) 138–143.
[5] B. Wang, Z.Q. Zheng, L.F. Zhu, Y.H. Yang, H.Y. Wu, Self-assembled and Pd decorated Zn_2SnO_4/ZnO wire-sheet shape nano-heterostructures networks hydrogen gas sensors, Sens. Actuators, B Chem. 195 (2014) 549–561.
[6] H. Tao, G.J. Fang, W.J. Ke, W. Zeng, J. Wang, In-situ synthesis of TiO_2 network nanoporous structure on Ti wire substrate and its application in fiber dye sensitized solar cells, J. Power Sources 245 (2014) 59–65.
[7] M. Sun, S. Zhang, T. Jiang, L. Zhang, J. Yu, Nano-wire networks of sulfur-polypyrrole composite cathode materials for rechargeable lithium batteries, Electrochem. Commun. 10 (2008) 1819–1822.
[8] W. Wang, M. Tian, Y. Wei, S.H. Lee, Y.C. Lee, R. Yang, Binder-free three-dimensional silicon/carbon nanowire networks for high performance lithium-ion battery anodes, Nano Energy 2 (2013) 943–950.
[9] N. Gao, W. Zhou, X. Jiang, G. Hong, T.-M. Fu, C.M. Lieber, General strategy for biodetection in high ionic strength solutions using transistor-based nanoelectronic sensors, Nano Lett. 15 (2015) 2143–2148.
[10] L. Xu, Z. Jiang, Q. Qing, L. Mai, Q. Zhang, C.M. Lieber, Design and synthesis of diverse functional kinked nanowire structures for nanoelectronic bioprobes, Nano Lett. 13 (2013) 746–751.
[11] J. Zhou, Y. Ding, S.Z. Deng, L. Gong, N.S. Xu, Z.L. Wang, Three-dimensional tungsten oxide nanowire networks, Adv. Mater. 17 (2005) 2107–2110.
[12] F. Zhao, X. Li, J. Zheng, X. Yang, F. Zhao, K.S. Wong, J. Wang, W. Lin, M. Wu, Q. Su, ZnO pine-nanotree arrays grown from facile metal chemical corrosion and oxidation, Chem. Mater. 20 (2008) 1197–1199.
[13] M.J. Bierman, Y.K.A. Lau, A.V. Kvit, A.L. Schmitt, S. Jin, Dislocation-driven nanowire growth and eshelby twist, Science 320 (2008) 1060–1063.
[14] T. Tada, K. Fukami, S. Nakanishi, H. Yamasaki, S. Fukushima, T. Nagai, S. Sakai, Y. Nakato, Tuning of the spacing and thickness of metal latticeworks by modulation of self-organized potential oscillations in tin (Sn) electrodeposition, Electrochim. Acta 50 (2005) 5050–5055.
[15] S. Nakanishi, K. Fukami, T. Tada, Y. Nakato, Metal latticeworks formed by self-organization in oscillatory electrodeposition, J. Am. Chem. Soc. 126 (2004) 9556–9557.
[16] J. Zhu, H. Peng, C.K. Chan, K. Jarausch, X.F. Zhang, Y. Cui, Hyperbranched lead selenide nanowire networks, Nano Lett. 7 (2007) 1095–1099.
[17] M. Abtew, G. Selvaduray, Lead-free solders in microelectronics, Mater. Sci. Eng. R Reports 27 (2000) 95–141.
[18] W.J. Boettinger, C.E. Johnson, L.A. Bendersky, K. Moon, M.E. Williams, G.R. Stafford, Whisker and hillock formation on Sn, Sn – Cu and Sn – Pb electrodeposits, Acta Mater. 53 (2005) 5033–5050.
[19] W.J. Choi, T.Y. Lee, K.N. Tu, N. Tamura, R.S. Celestre, A.A. MacDowell, Y.Y. Bong, L. Nguyen, Tin whiskers studied by synchrotron radiation scanning X-ray microdiffraction, Acta Mater. 51 (2003) 6253–6261.
[20] K.G. Compton, A. Mendizza, S.M. Arnold, Filamentary growths on metal surfaces – "whiskers", Corrosion 7 (1951) 327–334.
[21] F.C. Walsh, C. Ponce de León, Versatile electrochemical coatings and surface layers from aqueous methanesulfonic acid, Surf. Coatings Technol. 259 (2014) 676–697.
[22] S.W. Husain, M.S. Ahmed, I. Qamar, Dendritic morphology observed in the solid-state precipitation in binary alloys, Metall. Mater. Trans. A (1999) 1529–1534.
[23] Y.T. Hsieh, T.I. Leong, C.C. Huang, C.S. Yeh, I.W. Sun, Direct template-free electrochemical growth of hexagonal CuSn tubes from an ionic liquid, Chem. Commun. (Camb.) 46 (2010) 484–486.
[24] Y.T. Hsieh, I.W. Sun, Electrochemical growth of hierarchical CuSn nanobrushes from an ionic liquid, Electrochem. Commun. 13 (2011) 1510–1513.
[25] H. Han, J. Kim, H.S. Shin, J.Y. Song, W. Lee, Air-bridged ohmic contact on vertically aligned Si nanowire arrays: application to molecule sensors, Adv. Mater. 24 (2012) 2284–2288.
[26] E. Comini, G. Faglia, G. Sberveglieri, Z. Pan, Z. Wang, Stable and highly sensitive gas sensors based on semiconducting oxide nanobelts, Appl. Phys. Lett., 81 (2002) 1869–1871.
[27] F. Yang, Z. Guo, Tuning SnO_2 architectures with unitary or composite microstructure for the application of gas sensors, J. Colloid Interface Sci. 462 (2016) 140–147.
[28] D. Grujicic, B. Pesic, Electrodeposition of copper: the nucleation mechanisms, Electrochim. Acta 47 (2002) 2901–2912.
[29] M. Ibrahim, R. Radadi, Noncrystalline cobalt coatings on copper substrates by electrodeposition from complexing acidic glycine baths, Mater. Chem. Phys. 151 (2015) 222–232.
[30] National Institute for Materials Science, AtomWork (2010) http://crystdb.nims.go.jp/.
[31] D. Brandon, J. Pearson, W. Tozer, A single-crystal X-ray diffraction study of the ζ bronze structure, $Cu_{20}Sn_6$, Acta Crystallogr. B31 (1975) 774–779.
[32] H. Hendus, H. Knödler, Die Überstruktur der γ-Hochtemperaturphase in System Kupfer–Zinn, Acta Crystallogr. 9 (1956) 1036-1036.
[33] Y. Watanabe, Y. Fujinaga, H. Iwasaki, Lattice modulation in the long-period superstructure of Cu_3Sn, Acta Crystallogr. Sect. B Struct. Sci. 39 (1983) 306–311.
[34] B. Predel, Phase equilibria, crystallographic and thermodynamic date of binary alloys, in: O. Madelung (Ed.), Landolt-Börnstein Gr. IV Phys. Chem, Springer, 1994.
[35] R. Juškėnas, Z. Mockus, S. Kanapeckaitė, G. Stalnionis, A. Survila, XRD studies of the phase composition of the electrodeposited copper-rich Cu–Sn alloys, Electrochim. Acta 52 (2006) 928–935.
[36] A. Survila, Z. Mockus, S. Kanapeckaitė, V. Jasulaitienė, R. Juškėnas, Codeposition of copper and tin from acid sulphate solutions containing polyether sintanol DS-10 and micromolar amounts of halides, Electrochim. Acta 52 (2007) 3067–3074.
[37] M. Hasegawa, N. Yamachika, Y. Shacham-Diamand, Y. Okinaka, T. Osaka, Evidence for "superfilling" of submicrometer trenches with electroless copper deposit, Appl. Phys. Lett. 90 (2007) 1–4.
[38] M. Kang, M.E. Gross, A.A. Gewirth, Atomic force microscopy examination of Cu electrodeposition in trenches, J. Electrochem. Soc. 150 (2003) C292–C301.
[39] J.J. Kelly, A.C. West, Copper deposition in the presence of polyethylene glycol: I. Quartz crystal microbalance study, J. Electrochem. Soc. 145 (1998) 3472–3476.
[40] J.J. Kelly, A.C. West, Copper deposition in the presence of polyethylene glycol: II. Electrochemical impedance spectroscopy, J. Electrochem. Soc. 145 (1998) 3477–3481.
[41] K.R. Hebert, S. Adhikari, J.E. Houser, Chemical mechanism of suppression of copper electrodeposition by poly(ethylene glycol), J. Electrochem. Soc. 152 (2005) C324–C329.
[42] L. Bonou, M. Eyraud, R. Denoyel, Y. Massiani, Influence of additives on Cu electrodeposition mechanisms in acid solution: direct current study supported by non-electrochemical measurements, Electrochim. Acta 47 (2002) 4139–4148.
[43] N.M. Martyak, R. Seefeldt, Additive-effects during plating in acid tin methanesulfonate electrolytes, Electrochim. Acta 49 (2004) 4303–4311.
[44] N.D. Nikolić, K.I. Popov, L.J. Pavlović, M.G. Pavlović, Morphologies of copper deposits obtained by the electrodeposition at high overpotentials, Surf. Coatings Technol. 201 (2006) 560–566.